Open Access on 08/18/2015

ARTICLE

Core–Shell Nanoparticle-Based Peptide Therapeutics and Combined Hyperthermia for Enhanced Cancer Cell Apoptosis

Birju P. Shah,[†] Nicholas Pasquale,[†] Gejing De,[‡] Tao Tan,[‡] Jianjie Ma,[‡] and Ki-Bum Lee[†,*]

[†]Department of Chemistry and Chemical Biology, Rutgers, The State University of New Jersey, Piscataway, New Jersey 08854, United States, and [‡]Department of Surgery, Davis Heart and Lung Research Institute, The Ohio State University Wexner Medical Center, Columbus, Ohio 43210, United States

ABSTRACT Mitochondria-targeting peptides have garnered immense interest as potential chemotherapeutics in recent years. However, there is a clear need to develop strategies to overcome the critical limitations of peptides, such as poor solubility and the lack of target specificity, which impede their clinical applications. To this end, we report magnetic core–shell nanoparticle (MCNP)-mediated delivery of a mitochondria-targeting pro-apoptotic amphipathic tail-anchoring peptide (ATAP) to malignant brain and metastatic breast cancer cells. Conjugation of ATAP to the MCNPs significantly enhanced the chemotherapeutic efficacy of ATAP, while the presence of targeting ligands afforded selective delivery to cancer cells. Induction of MCNP-mediated hyperthermia further potentiated the efficacy of ATAP. In summary, a combination of MCNP-mediated ATAP delivery and subsequent hyperthermia resulted in an enhanced effect on mitochondrial dysfunction, thus resulting in increased cancer cell apoptosis.

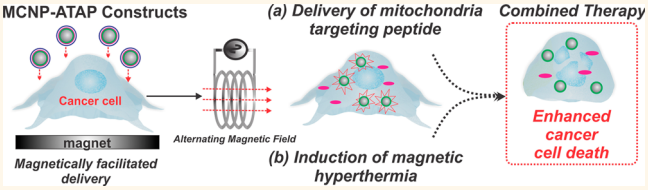

KEYWORDS: magnetic core–shell nanoparticle · mitochondria-targeting peptide · amphipathic tail-anchoring peptide · magnetic hyperthermia · magnetically facilitated delivery · combined therapy

The outstanding progress made in fundamental cancer biology over the past decades has not yet fully translated into comparable clinical advances.[1,2] This has been mainly attributed to inadequacies of approaches available to administer the therapeutics moieties, such that they will reach the target tumor site in their most potent form with minimal collateral damage.[3] To overcome this challenge, it is crucial to develop advanced methods that can synergistically achieve three main goals: (i) provide the means to overcome any physiological barriers preventing the access of therapeutics to the target tumor or cellular site,[4,5] (ii) increase the target selectivity of the therapeutic moieties,[6] and (iii) enhance their chemotherapeutic efficacy by combining them with other adjuvant treatment modalities.[1,7]

While tumor and cellular targeting of chemotherapeutics has been widely demonstrated to improve their efficacy,[4,6] subcellular organelles such as the nucleus and mitochondria are also quickly gaining interest as chemotherapeutic targets, since any damage to these organelles leads to efficient and irreversible cell death.[8,9] Of particular importance are mitochondria, which have been shown to be intricately linked to tumor progression and chemoresistance seen in cancer stem cells, in addition to playing an important role in cellular apoptosis.[10,11] Toward this, several therapeutic moieties, such as small molecules, peptides, and RNA-interference (RNAi) molecules, capable of inducing mitochondria-dependent cell death, have been developed as new strategies for cancer therapy.[12–15] Among these, peptides are considered an attractive option, as they are not only capable of endogenous high-affinity interactions with mitochondria to initiate apoptosis but are also more readily delivered to the cells.[16]

One such example of a novel mitochondrial targeting peptide is amphipathic tail-anchoring peptide (ATAP), which has been shown to trigger potent mitochondria-dependent apoptosis.[17] ATAP selectively targets

* Address correspondence to kblee@rutgers.edu.

Received for review June 24, 2014 and accepted August 18, 2014.

Published online August 18, 2014
10.1021/nn503431x

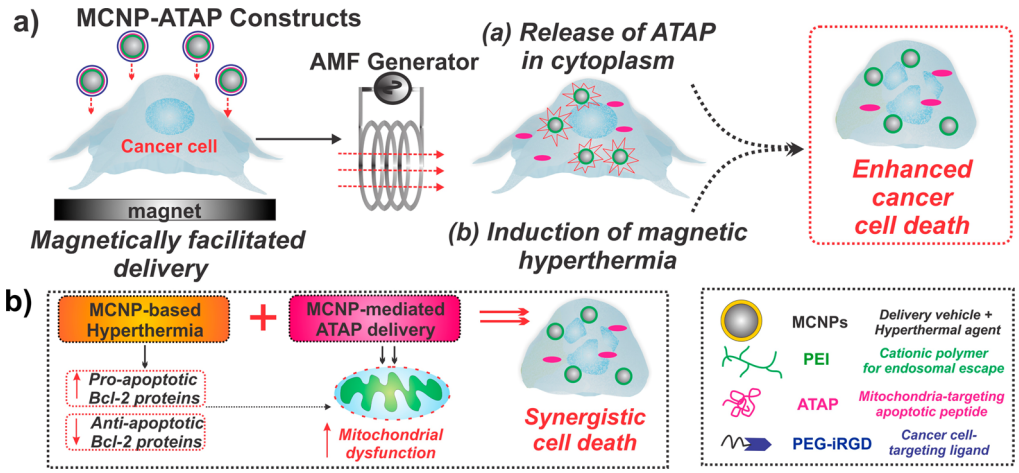

Figure 1. (a) Schematic diagram depicting magnetically facilitated targeted delivery of MCNP-ATAP to brain and breast cancer cells, wherein the release of ATAP from the MCNPs in the cytoplasm coupled with induction of magnetic hyperthermia in the presence of an alternating magnetic field (AMF) can result in synergistic cell death. (b) MCNP-based hyperthermia can result in inactivation of anti-apoptotic bcl-2 proteins, with a concomitant increase in the pro-apoptotic bcl-2 proteins, thus sensitizing the cancer cells toward apoptosis. On the other hand, MCNP-ATAP constructs permeabilize the outer mitochondrial membrane and thus induce mitochondrial dysfunction. Such a combined therapy can synergistically enhance cancer cell death. MCNP, magnetic core–shell nanoparticles; PEI, polyethylenimine; ATAP, amphipathic tail-anchoring peptide; PEG, polyethylene glycol; iRGD, internalizing RGD.

mitochondria and induces cytochrome *c* release through the perturbation of mitochondrial membrane permeability, thus initiating an irreversible cascade of biochemical changes finally resulting in apoptosis.[18] More importantly, unlike other mitochondria-targeting peptides, the cytotoxic effects of ATAP do not require the presence of pro-apoptotic proteins nor are they influenced by the concentration of anti-apoptotic proteins, which are often mutated in neoplasms, thus making ATAP a novel and an attractive therapeutic moiety for the treatment of various types of cancers.[17−19] However, the widespread clinical applications of ATAP and other mitochondria-targeting peptides are hampered by two key limitations: (i) poor aqueous solubility and stability under physiological conditions due to their amphipathic structure and (ii) lack of tumor-targeting capabilities.[16,20] Hence, prior to their clinical application, it is important to develop strategies that can not only improve the biopharmaceutical properties of these peptides but also ensure their recognition and penetration specifically into tumor cells.[19−21]

In this regard, nanoparticle-based approaches by virtue of their unique nanoscale and physicochemical properties (*e.g.*, multivalent drug delivery) have been shown to overcome the aforementioned challenges by providing means to improve delivery and drug efficacy. Moreover, they also allow for the incorporation of additional functionalities, such as hyperthermia, imaging, and photothermal therapy, based upon their unique compositions.[22,23] For instance, magnetic nanoparticles (MNPs) not only can be used as MRI contrast agents but can also afford localized increase in temperature (known as hyperthermia) in the presence of an alternating magnetic field.[24,25] Such localized hyperthermia has been demonstrated to sensitize tumors to chemotherapy and radiation therapy and hence is considered to be an attractive adjuvant therapy.[26,27] More importantly, hyperthermia has also been shown to further enhance the pro-apoptotic ability of peptides and other therapeutics by directly activating the pro-apoptotic and inhibiting anti-apoptotic Bcl-2 family members,[28] as well as increase the permeabilization of the mitochondrial membrane.[29−31] Additionally, our group as well as others have recently demonstrated that these MNPs can be further modified with a gold shell, thus having both magnetic and plasmonic properties that can be utilized for various biological applications including cell targeting, imaging, and chemotherapy.[32]

To this end, we describe the development of magnetic core–shell nanoparticles (MCNP) for the efficient delivery of ATAP and localized hyperthermia for enhanced apoptosis in cancer cells (Figure 1). As a proof-of-concept, we tested the efficacy of our MCNP-ATAP constructs in malignant brain cancer cells (glioblastoma multiforme, U87vIII) and metastatic breast cancer cells (MDA-MB-231), which contain a subpopulation of cancer stem cells.[33] Owing to their unique composition, our MCNPs performed multiple functions, as demonstrated below. First, the gold shell allowed for facile conjugation of ATAP and a tumor targeting peptide (iRGD),[6] thereby affording tumor-targeting capability to our MCNP-ATAP constructs. Second, the magnetic core allowed for magnetically facilitated delivery of the MCNP-ATAP constructs, thus leading to enhanced cellular uptake.[32,34,35] In addition, the magnetic core of the MCNPs enabled induction of localized hyperthermia,[36] which could act in a complementary fashion with the ATAP moieties to synergistically enhance cancer cell apoptosis. Thus, we hypothesized that our MCNPs

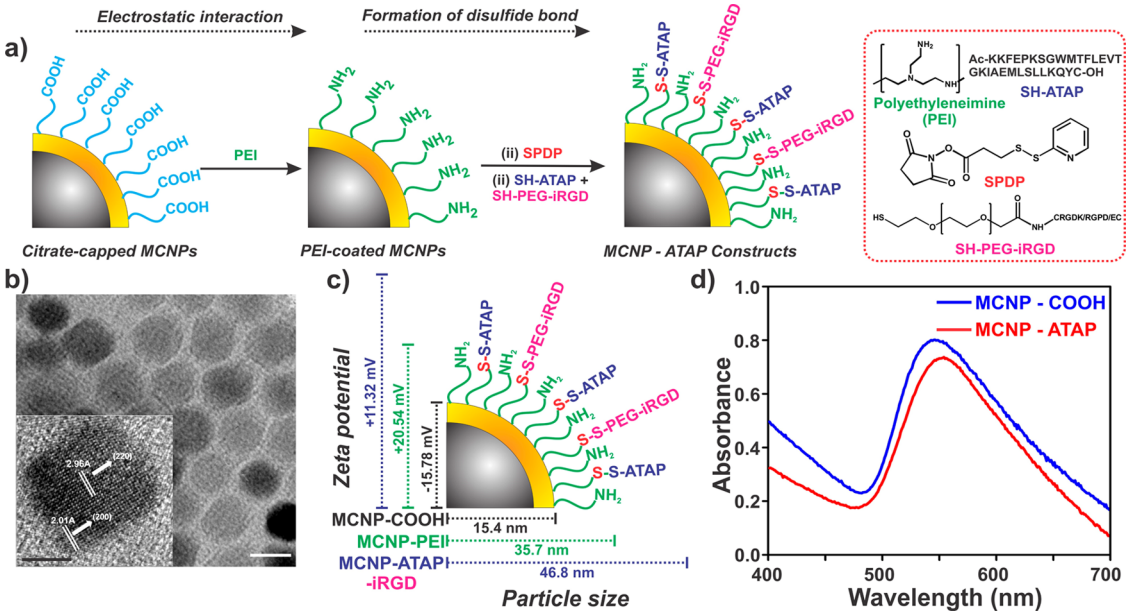

Figure 2. (a) Conjugation of ATAP and targeting ligands to MCNPs. PEI, polyethylenimine; ATAP, amphipathic tail-anchoring peptide; SPDP, *N*-succinimidyl 3-(2-pyridyldithio)propionate; PEG, polyethylene glycol; iRGD, internalizing RGD. (b) TEM images of the MCNP-ATAP constructs. High-resolution TEM images of MCNPs (inset) show crystalline lattices of Fe and Au. Scale bar is 20 nm (inset 5 nm). (c) Hydrodynamic diameter and zeta potential measurements at each step of formation of MCNP-ATAP constructs. (d) UV−visible spectroscopy analysis of MCNPs before and after conjugation with ATAP.

would serve as a versatile platform enabling the application of two orthogonal yet complementary modalities, thereby resulting in significant improvements in cancer therapy.

RESULTS

Synthesis and Characterization of MCNP-ATAP Conjugates. As a first step toward synthesizing MCNP-ATAP constructs (Figure 2a), the magnetic cores were synthesized by making slight modifications to a previously reported protocol.[37] Then, citrate-capped MCNPs were synthesized according to previously reported methods with slight modifications.[32] The as-synthesized citrate-capped MCNPs were found to have a hydrodynamic diameter of 15.4 nm (Figure 2b). Thereafter these MCNPs were coated with branched polyethylenimine (PEI, MW = 10 kDa) *via* electrostatic interactions to afford an overall positive charge to the complex. Additionally, PEI is known to act as a proton sponge and induce endosomolysis within the cytoplasm,[38] such that the MCNP-ATAP constructs will not be subjected to the highly acidic endosomal environment and be released within the cytoplasm in their most potent form. Subsequently, these amine-terminated MCNPs were coupled to the thiol-terminated ATAP moieties *via* a heterobifunctional cross-linker, *N*-succinimidyl 3-(2-pyridyldithio)propionate (SPDP), to form redox-responsive MCNP-ATAP constructs. Additionally, thiol-PEG moieties bearing targeting moieties (iRGD)[6] were also conjugated to the MCNPs using the SPDP linker to improve the overall aqueous solubility of the MCNP-ATAP constructs and to allow for selective delivery of MCNP-ATAP constructs to U87 glioblastoma cells, which contain upregulated levels of integrins.[39]

The particle diameter and zeta potential of the MCNP-ATAP constructs was measured using dynamic light scattering after each step of conjugation (Figure 2c). The final MCNP constructs had a hydrodynamic diameter of 46.8 ± 2.3 nm and were positively charged (ζ = +15.78 mV) to allow for increased cellular uptake. Additionally, these MCNP-ATAPs showed a slight red shift in the characteristic surface plasmon resonance band as compared to unconjugated MCNPs, thus confirming the presence of ATAP moieties on the surface (Figure 2d).[40] The amount of ATAP present on the MCNPs was quantified by measuring the concentration of the unconjugated ATAP moieties present in the supernatant using UV−vis spectroscopy (Experimental Section). Approximately, 50% of the loading amount of ATAP was conjugated on the nanoparticles and it was found that 10 nM ATAP was present per 1 μg/mL of MCNPs (~500 ATAP molecules per NP). The synthesized MCNPs were also found to be biocompatible within a wide range of concentrations (5−50 μg/mL) and did not affect the cell viability in either U87vIII or MDA-MB-231 cells (Supporting Information, Figures S1 and S2). Additionally, we tested the biocompatibility of MCNPs coated with PEI (to mimic the conditions found after the cleavage of disulfide bond and subsequent release of ATAP within the cytoplasm) and found that these MCNP-PEI constructs also did not induce any noticeable cytotoxicity at the concentrations present in U87vIII cells (Supporting Information, Figure S3).

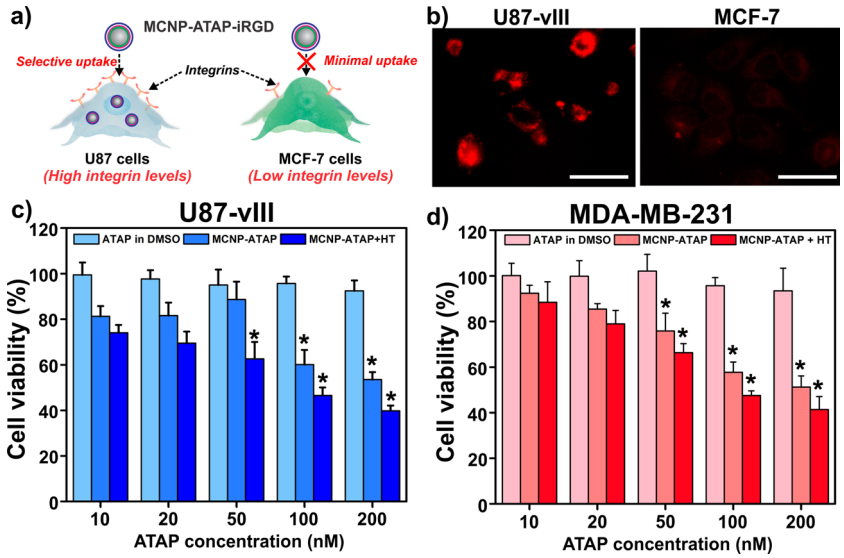

Figure 3. (a) internalizing RGD (iRGD)-modified MCNP-ATAP constructs are delivered specifically to U87 cells (having high levels of integrins) as compared to MCF-7 cells (having low levels of integrins), due to increased receptor−ligand interactions between iRGD and integrins expressed on U87 cell membrane. (b) Epifluorescent images depicting targeted delivery of iRGD modified MCNP-ATAP constructs to integrin-positive U87 and integrin-negative MCF-7 cells. (c) Cell viability of MCNP-ATAP treated U87vIII cells in the presence and absence of hyperthermia 48h post transfection, using MTS-based cell proliferation assay. Concentration of ATAP in DMSO and on the MCNPs was 200 nM. MCNP concentration was 20 μg/mL. Magnetic hyperthermia was induced for 45 min. * indicates $p < 0.01$. d) Cell viability of MCNP-ATAP treated MDA-MB-231 cells in the presence and absence of hyperthermia 48 h post transfection, using MTS-based cell proliferation assay. Concentration of ATAP in DMSO and on the MCNPs was 200 nM. MCNP concentration was 20 μg/mL. Magnetic hyperthermia was induced for 45 min. * indicates $p < 0.01$.

Integrin-Mediated Targeted Delivery of MCNP-ATAP Constructs to Cancer Cells. Once the MCNP-ATAP constructs were generated and characterized, we then went on to test their targeted delivery and the subsequent apoptotic efficacy in brain cancer cells (U87vIII) overexpressing the mutant epidermal growth factor receptor vIII (EGFRvIII).[41] The overexpression of EGFRvIII has been implicated in enhancing the tumorigenicity and resistance to radiation and chemotherapy in GBM.[42] As mentioned earlier, ATAP lacks a tumor targeting moiety, thereby restricting its widespread clinical application. Hence, we modified the carboxyl end-groups of the PEG chains, with a targeting ligand, iRGD, which has been reported to home to the $\alpha v\beta 3$ integrin surface receptors present in glioblastoma and other cancer cells (Figure 3a).[43] These iRGD-grafted PEG chains were then conjugated on the surface of MCNPs as described in the Experimental Section. Additionally, we conjugated a fluorophore (Alexa Fluor 594) on the surface of the MCNPs to make them amenable for visualization using fluorescence microscopy. The iRGD-conjugated MCNPs were then incubated with U87vIII and MCF-7 (breast cancer) cells, which have low integrin expression;[44] the cells were then washed thrice with PBS to remove any excess MCNPs and thereafter imaged using fluorescence microscopy. As seen in Figure 3b, U87vIII cells, having higher integrin levels show significantly higher uptake of the iRGD conjugated MCNPs as compared to MCF-7 cells, which have low levels of integrins. Taken together, these results indicate that by simply conjugating targeting ligands on the surface of the MCNPs, we can adopt a facile approach for conferring tumor targeting capability to the ATAP moieties without making any structural modifications to ATAP, which can compromise its activity.

Apoptotic Efficacy of MCNP-ATAP Constructs in Cancer Cells. We next tested the apoptotic capability of these MCNP-ATAP constructs in both glioblastoma (U87vIII) and breast cancer (MDA-MB-231) cells. Prior to testing MCNP-ATAP constructs, we first tested the effect of varying concentrations of unconjugated ATAP (in DMSO) on the viability of U87vIII and MDA-MB-231 cells using the MTS assay (Supporting Information, Figure S4). Consistent with our previous study,[18] the unconjugated ATAP (in DMSO) had negligible effect on the viability of both cell lines, even at significantly higher ATAP concentrations ([ATAP] = 200 nM); Figure 3c). Next, we tested the chemotherapeutic efficacy of MCNP-ATAP constructs delivered to brain and breast cancer cells using magnetically facilitated delivery.[35,45] We first optimized the duration of magnetic field exposure (Supporting Information, Figure S5) and found that 30 min was the optimal exposure time, resulting in significantly higher uptake of MCNP-ATAP constructs. We then tested the apoptosis-inducing ability of MCNP-ATAP constructs in U87vIII and MDA-MB-231 cells by delivering varying concentrations of MCNP-ATAP constructs (Figure 3c and d) to cells using magnetically facilitated delivery (30 min magnetic field exposure). The viability of the

treated cells was then determined using the MTS assay 48 h post-transfection. As can be seen from Figure 3c,d, MCNP-ATAP constructs led to a significant increase in cell death, as compared to unconjugated ATAP at all concentrations in both U87vIII and MDA-MB-231 cells. Taken together, these results indicate that the potency of ATAP is greatly enhanced when conjugated to MCNPs, possibly due to an increase in its aqueous solubility in the presence of PEG molecules. Additionally, we tested whether release of ATAP from the MCNPs was required to achieve a maximal effect on cell viability. For this purpose, we compared the effect of cell viability of the above-mentioned MCNP-ATAP constructs (with a cleavable disulfide bond) with MCNP-ATAP constructs (with a noncleavable amide bond) in brain cancer cells. From this, it is clearly evident that MCNP-ATAP constructs with the noncleavable amide bond show a modest decrease in the cell viability as compared to the cleavable constructs (Supporting Information, Figure S6). Taken together, these results suggest that while the conjugation of ATAP to the MCNPs increases its overall chemotherapeutic efficacy, release of ATAP from the MCNPs is essential to achieve the maximal apoptotic effect.

Effect of MCNP-Mediated Combined ATAP Delivery and Hyperthermia in Cancer Cells. As mentioned earlier, our MCNPs could induce localized hyperthermia in the presence of an AMF, which can act in a synergistic manner with the ATAP moieties to increase the permeabilization of the mitochondrial membrane and thus enhance apoptosis (Figure 1b).[28,29] Hence, we wanted to evaluate whether the combination of MCNP-mediated hyperthermia and ATAP delivery would lead to a synergistic enhancement of cancer cell apoptosis. However, prior to testing the MCNP-mediated magnetic hyperthermia, we tested the combination therapy of MCNP-ATAP and water-bath hyperthermia. The MCNP-ATAP-treated cells were exposed to 45 min of water-bath hyperthermia (43 °C), and the percent cell viability was quantified as before. Combined treatment of water-bath hyperthermia with MCNP-ATAP constructs did not lead to significant increase in cancer cell apoptosis (Supporting Information, Figure S7). Hence, in the next step, we tested the combination therapy of MCNP-mediated magnetic hyperthermia and ATAP delivery. We first optimized the duration of hyperthermia by exposing the cells transfected with MCNPs to either 15, 30, 45, or 60 min of hyperthermia (Supporting Information, Figure S8). From this, it was found that 45 min of hyperthermia was optimal to induce further cell death (an additional ~20% based on MTS), and further increases in the exposure time did not lead to a corresponding increase in cell death. Thereafter, we tested the combined therapy by incubating the U87vIII and MDA-MB-231 cells with MCNP-ATAP constructs and inducing hyperthermia 24 h post-transfection. The cell viability following the combined therapy was determined 48 h post-transfection using an MTS cell viability assay. From Figure 3c, it can be seen that the combined therapy of MCNP-ATAP ([ATAP] = 200 nM) and hyperthermia (45 min) caused significant cell death, as compared to either treatment alone. Collectively, these results support our hypothesis that hyperthermia can significantly enhance ATAP-mediated cell death. In addition, these results also clearly suggest that such an enhancement in cell death can only be seen in the case of MCNP-mediated hyperthermia and ATAP delivery, as compared to water-bath hyperthermia.

Effect of MCNP-ATAP Constructs on Mitochondrial Depolarization of Cancer Cells. In order to confirm that the apoptotic effect of MCNP-ATAP constructs was caused as a result of mitochondrial dysfunction, we investigated the loss of mitochondrial membrane potential ($\Delta\Psi$m), using a flow-cytometry-based JC-1 assay.[11] Mitochondrial depolarization occurs as a result of mitochondrial dysfunction and is regarded as a hallmark of apoptosis (Figure 4a). JC-1 is a lipophilic, cationic dye, which selectively translocates to the mitochondria and undergoes a color change as a function of the mitochondrial membrane potential ($\Delta\Psi$m).[46] In healthy cells with high $\Delta\Psi$m, JC-1 spontaneously forms intense red colored complexes known as J-aggregates, whereas in apoptotic cells with low $\Delta\Psi$m, JC-1 remains in the green monomeric form.[47] From Figure 4b, it can be seen that there is no obvious change in mitochondrial membrane potential in U87vIII cells treated with MCNPs alone, as is evident from the formation of red J-aggregates (96.0%) with minimal green JC-1 monomers (2.6%). When the U87 cells are treated with MCNP-ATAP, there is a dramatic increase in the green fluorescence (JC-1 monomer in the cytoplasm, 25.7%), suggesting increased mitochondrial depolarization and hence apoptosis. This is also coupled with a decrease in red fluorescence (normal mitochondria, 67.0%). Taken together, these results suggest that the MCNP-mediated delivery of ATAP resulted in significantly higher mitochondrial dysfunction and eventually increased apoptosis, as compared to unconjugated ATAP (Supporting Information, Figure S9). Furthermore, when hyperthermia is induced in cells treated with MCNP-ATAP, it causes a further increase in the green fluorescence (38.1%, as compared to 25.7% seen with MCNP-ATAP), thus suggesting the enhanced effect of hyperthermia (HT) on the mitochondrial-regulated apoptosis caused by ATAP, because of their cooperative mechanism of action. To further quantify the ATAP-induced mitochondria-dependent apoptosis of U87 cells, we conducted a flow-cytometry-based annexin V-FITC/PI assay (Supporting Information, Figure S10). Combined treatment of MCNP-mediated ATAP and hyperthermia (MCNP-ATAP+HT) showed the highest percentage of apoptotic cells (38.3%), as compared to the individual MCNP-ATAP only and MCNP-induced hyperthermia treatments.

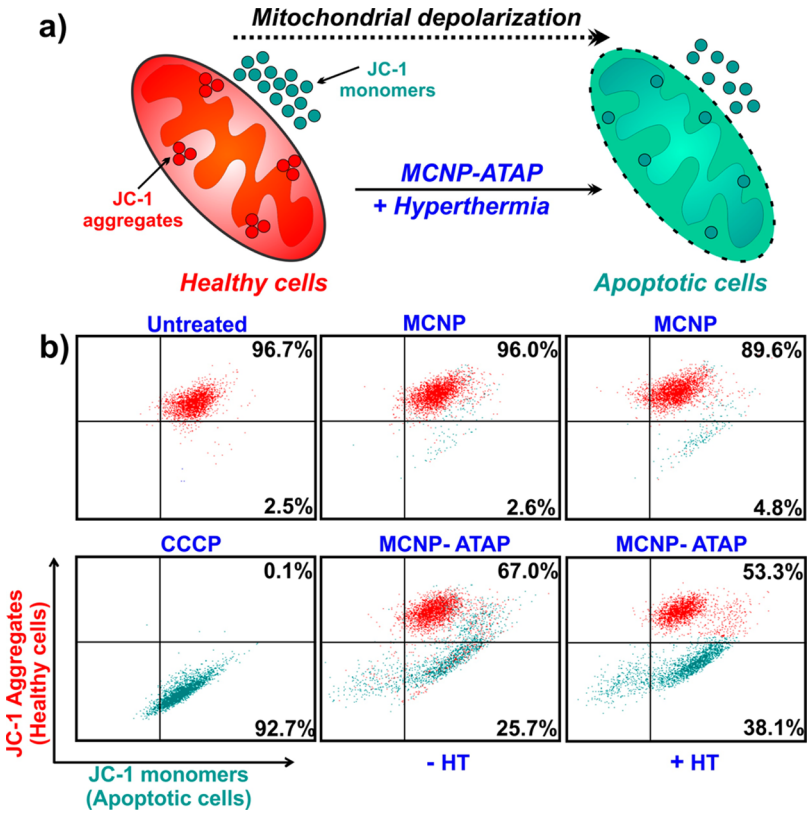

Figure 4. (a) Schematic diagram depicting the presence of JC-1 aggregates (red; healthy cells) and JC-1 monomers (green; apoptotic cells) as a result of combined MCNP-ATAP and hyperthermia treatment. (b) Flow-cytometry-based JC-1 assay as a measure of mitochondrial depolarization induced by MCNP-ATAP constructs. The top right quadrant indicates normal mitochondria (healthy cells, red fluorescence), whereas the bottom right quadrant indicates depolarized mitochondria (apoptotic cells, green fluorescence). CCCP, carbonyl cyanide 3-chlorophenylhydrazone (positive control); MCNP, 20 μg/mL; ATAP, 100 nM; hyperthermia (HT), 45 min.

Preliminary *in Vivo* Testing of ATAP-iRGD Constructs. Once we established that the potency of ATAP increases exponentially upon conjugation to MCNPs, we then went on to test the potency of MCNP-ATAP constructs *in vivo* using a mouse xenograft model. Since such peptide–nanoparticle constructs are administered systemically in repeated dosages in a clinical setting, it is therefore essential to identify the potential of these constructs to induce an immune response in the mice. We therefore systemically injected MCNP-ATAP-IRGD constructs in mice and found that the constructs show no obvious immunogenicity when tested over a period of 3 weeks. In addition, we tested the tumor-targeting capability of ATAP-iRGD constructs in an esophageal cancer (KYSE)[48] xenograft model. These studies showed that ATAP-iRGD had similar tumor suppression effects to those of BH3-iRGD peptide (equal molar concentration), thus indicating ATAP-iRGD suppresses esophageal tumor growth with limited off-target toxicity in the mouse model (Supporting Information, Figure S11). While the IC_{50} for ATAP-iRGD was found to be 4–5 μM, after MCNP packaging of ATAP, we found that MCNP-ATAP remarkably improved the IC_{50} from the μM range to the 50 nM range in the MTT assay. Although these *in vivo* experiments are still in the preliminary stage, these *in vivo* results strongly suggest the potential of MCNPs to enhance the delivery and efficacy of ATAP in tumors.

CONCLUSION

In conclusion, our MCNP-based targeted delivery of ATAP combined with magnetic hyperthermia leads to significantly enhanced apoptosis as a result of their synergistic effect on mitochondrial dysfunction in both malignant brain cancer and metastatic breast cancer cells. By modifying these MCNPs with PEG molecules and targeting ligands such as iRGD, we were also able to overcome the critical obstacles impeding the clinical applications of ATAP as a cancer therapeutic, namely, poor aqueous solubility and lack of tumor-homing capacity. Most importantly, our MCNPs afforded us the dual capabilities of effectively delivering and releasing the ATAP moieties as well as inducing localized hyperthermia, thereby potentiating the chemotherapeutic efficacy of ATAP. Additionally, our nanoparticle platform can also afford noninvasive tracking of cells using MRI (due to the magnetic core) and dark-field imaging (due to the gold shell) and, hence, afford complementary information for therapy and diagnosis. Our study represents a proof-of-concept demonstration of conjugation of ATAP molecules on the

surface of MCNPs and the downstream effects of these constructs on cellular processes such as mitochondrial permeabilization and apoptosis. We are currently continuing to evaluate the chemotherapeutic efficacy of the combined therapy in xenograft models.

METHODS

Synthesis of Core–Shell Nanoparticles. *Synthesis of Zn-Doped Iron Oxide Nanoparticles.* In a typical experiment for synthesis of the nanoparticles,[49] 1 mmol of zinc chloride ($ZnCl_2$), 2 mmol of iron(III) acetylacetonate ($Fe(acac)_3$, $C_{15}H_{21}FeO_6$), 6 mmol of oleic acid, 6 mmol of oleylamine, and 10 mmol of 1,2-hexadecanediol were mixed in 20 mL of trioctylamine in a 100 mL three-neck round-bottom flask. The reaction mixture was heated to 200 °C for 2 h, after which the temperature was increased to 300 °C. After 1 h, the reaction mixture was cooled to room temperature and the magnetic nanoparticles were precipitated using ethanol. They were purified by repeated centrifugation and sonication. The as-obtained nanoparticles were then dried overnight under vacuum.

Synthesis of Au-Coated Magnetic Nanoparticles. In a typical coating experiment,[37] 2.5 mg of zinc-doped iron oxide nanoparticles in chloroform were added to 10 mL of tri-*n*-octylamine and heated in order to evaporate the chloroform. After cooling the solution to room temperature, 15 μL of a gold stock solution (5 mg of $HAuCl_4$ in 300 μL of ethyl acetate) was added slowly dropwise to the reaction vial followed by 0.306 μL of 1-dodecanethiol. The reaction mixture was heated to 150 °C and kept at this temperature for 4 h. The Au-coated nanoparticles were centrifuged and washed several times with chloroform *via* centrifugation and magnetic decantation to separate pure gold nanoparticles from core–shell nanoparticles

Synthesis of Water-Soluble Core–Shell Nanoparticles. For converting the hydrophobic core–shell nanoparticles into hydrophilic ones, a ligand exchange reaction was carried out by sonicating the hydrophobic MCNPs in the presence of trisodium citrate and TMAOH.[50] In a typical experiment, the particles were suspended in a minimal amount of chloroform and added to 5 mL of 1 M TMAOH containing 0.06 g of trisodium citrate. A few drops of acid were added to ensure slightly acidic conditions. The resulting suspension was sonicated on a probe-type sonicator for 30 min. The resulting solution was purified by multiple rounds of magnetic decantation.

Formation of MCNP-ATAP Complexes. To obtain PEI-coated MNPs, the water-soluble MNPs from above were first diluted with DPBS to reach a final concentration of 0.1 mg/mL. Afterward, excess 10 kDa branched PEI (Sigma-Aldrich) was added dropwise (1 mg/mL). After spinning overnight, the PEI-coated MNPs were filtered using a centrifugal filter unit (EMD Millipore, 10 000 MW). Thereafter, the PEI-coated MNPs were mixed with heterobifunctional linker and SPDP (0.1 mM) and incubated at room temperature for 4–6 h with continuous shaking. Simultaneously, SH-PEG-COOH moieties were linked to iRGD-NH_2 moieties using EDC coupling. Thereafter, varying ratios of thiolated ATAP and thiolated PEG-iRGD constructs were added to the thiol-reactive SPDP-linked MCNP-PEI complexes. The resulting mixture was allowed to react overnight, followed by purification using centrifugation. The resulting MCNP-ATAP complexes were then dispersed in sterile DPBS (Dulbecco's Phosphate Buffered Saline) for further use. For targeted delivery, the MCNP-PEI complexes were also conjugated with Alexa-Fluor594-succinimide to allow for monitoring the uptake of MCNP constructs using fluorescence microscopy.

Quantification of ATAP Conjugated to MCNPs Using UV–Visible Spectroscopy. A standard curve of ATAP (in 8 M urea) was constructed by measuring the absorbance of different concentrations of ATAP solutions at 280 nm using a UV–visible spectrometer (Cary US). The amount (in milligrams) of ATAP present per milliliter of solution was then calculated by using the following equation:

$$\text{mg ATAP per mL} = (\text{A280} \times \text{Dilution Factor} \times \text{MW}) / [(1 \times 5560) + (1 + 1200)]$$

In order to calculate the amount of ATAP conjugated per milligram of MCNP, the MCNP-ATAP constructs were incubated with 0.1 M DTT solution to cleave the disulfide bonds between MCNP and ATAP. The solution was centrifuged, and the supernatant collected. The amount of ATAP per milligram of MCNP was then calculated using the above equation by measuring the absorbance at A280 nm.

Particle Size and Zeta Potential Analysis. Dynamic light scattering (DLS) and zeta potential analyses were performed using a Malvern Instruments Zetasizer Nano ZS-90 instrument (Southboro, MA, USA) with reproducibility being verified by collection and comparison of sequential measurements. Complexes (MCNP, MCNP-PEI, and MCNP-ATAP) for DLS and zeta potential measurements were prepared using purified water (resistivity = 18.5 MΩ-cm). DLS measurements were performed at a 90° scattering angle at 25 °C. *Z*-Average sizes of three sequential measurements were collected and analyzed. Zeta potential measurements were collected at 25 °C, and the *Z*-average potentials following three sequential measurements were collected and analyzed.

Cell Culture. U87-EGFRvIII cells were cultured in DMEM (Dulbecco's modified Eagle's medium) with high glucose (Invitrogen), 10% fetal bovine serum (FBS), 1% streptomycin–penicillin, 1% Glutamax (Invitrogen), and hygromycin B (30 μg/mL), while MDA-MB-231 and MCF-7 cells were cultured in DMEM/F-12 with 10% FBS, 1% streptomycin–penicillin, and 1% Glutamax.

Magnetically Facilitated Delivery of MCNPs. Twenty-four hours before the magnetically facilitated delivery of MCNPs, 2×10^5 cells in a volume of 500 μL were seeded into each well of a 24-well plate, so as to attain 80–90% confluency at the time of transfection. For the transfection of MCNP-ATAP constructs, the varying amounts of MCNP-ATAP constructs were gently mixed with OptiMEM and then were added to each well to obtain the desired MCNP-ATAP concentration per well. Subsequently, the cell culture plates were placed on the Nd–Fe–B magnetic plates (OZ Biosciences, France) for 15 min. Following this, the cells were transferred back to the incubator and the media was replaced with growth medium after 1–2 h of additional incubation.

Cytotoxicity Assays. The percentage of viable cells was determined by MTS assay following standard protocols described by the manufacturer. All experiments were conducted in triplicate and averaged. Forty-eight hours after initial transfection, the MTS data are represented as formazan absorbance at 490 nm, considering the control (untreated) cells as 100% viable.

Targeted Delivery. Highly tumorigenic U87-EGFRvIII cells and low-tumorigenic MCF-7 cells were cultured in 24-well plates, at a density of 5×10^4 cells per well. For MCF-7 cells, the normal growth media was DMEM/F-12 (with high glucose, Invitrogen), 10% FBS, 1% Glutamax, and 1% penicillin–streptomycin. For the delivery of iRGD-conjugated MCNPs, media was exchanged with serum-free DMEM media, and the cells were incubated with iRGD-MCNPs for 6–8 h. Fluorescence images were taken after replacing the serum-free media with regular media.

Magnetic Hyperthermia. Twenty-four hours after seeding cells as described above, varying concentrations (5–20 μg/mL) of MCNP-ATAP constructs were prepared in OptiMEM (Life Technologies) and added to each well. Subsequently, the cell culture plates were exposed to magnetofection for 15 min as described above. The culture plates were placed back into the incubator for 1 h, and afterward, the cells were washed with DPBS and the transfection medium was replaced with fresh growth medium. Twenty-four hours after transfection, cells were washed with DPBS, trypsinized, and exposed to an alternating magnetic field (5 kA/m, 300 kHz) for the desired amount of time. Thereafter, fresh media was added to the treated cells and the cells were plated back into 12-well plates.

Measurement of Mitochondrial Membrane Potential. Mitochondrial stability was assessed by flow cytometry after incubation with 5,59,6,69-tetrachloro-1,19,3,39-tetraethylbenzimidoazolylcarbocyanino iodide (JC-1; Molecular Probes, Eugene, OR, USA) as per the manufacturer's recommended protocol. Briefly, the cells were analyzed using flow-cytometry-based JC-1 assay 48 h after initial transfection. The cells were trypsinized, resuspended in warm DPBS, and incubated with JC-1 (2 μM) for 15−30 min at 37 °C and 5% CO_2. Thereafter the cells were centrifuged, resuspended in 500 μL of PBS, and analyzed immediately on a flow cytometer (Gallios, Beckman Coulter, Inc.) with 488 nm excitation using emission filters appropriate for Alexa Fluor 488 dye (520 nm) and R-phycoerthyrin (590 nm). Standard compensation was performed using the carbonyl cyanide 3-chlorophenylhydrazone (CCCP)-treated cells as positive control. Untreated cells (no MCNP and no ATAP) were used as negative controls.

Apoptosis Assay. To assay apoptosis using annexin V-FLUOS and propidium iodide staining (Roche), 48 h after initial transfection, 10^6 cells were prepared in 1 mL of PBS with 10% FBS in each test tube. After centrifugation, cells were resuspended in 100 μL of annexin V binding buffer (ice-cold), and annexin V-FLUOS and propidium iodide (PI) were added following the manufacturer's recommendation. Samples were incubated in the dark for 15 min at room temperature. Finally, 400 μL of additional ice-cold annexin V binding buffer was added, and the samples were kept on ice under foil until analysis using flow cytometry (Gallios, Beckman Coulter, Inc.). Early apoptotic cells with exposed phosphatidylserine but intact cell membranes bound to annexin V-FITC but excluded propidium iodide. Cells in necrotic or late apoptotic stages were labeled with both annexin V-FITC and propidium iodide.

Xenograft Studies in Nude Mice. Handling of animals was performed in accordance with protocols approved by the Institutional Animal Care and Use Committee (IACUC) of the The Ohio State University. Five-week-old NCR nude mice (Taconic Farms, Germantown, NY, USA) were implanted subcutaneously in both flanks with 2 × 106 KYSE cells. After tumors reached 4 to 7 mm in diameter (about 9−14 days after implantation), the mice were randomly divided into two groups so that both the mean and the variance of the tumor diameters are of no significant difference among the groups prior to treatment. The ATAP-iRGD-M8 peptide was injected through the tail vein once every 2 days during the whole procedure. Tumor volume was measured by a digital caliper (Thermo Fisher Scientific, Waltham, MA, USA). Tumor volume was determined from the orthogonal dimensions (length, width) using the following formula: tumor volume = $^1/_2$(length × width^2). According to the IACUC guideline, the experiments were terminated when tumors reached 1.5 cm in diameter. At the end of the experiment, mice were sacrificed and xenografts were removed and weighed. For toxicological evaluation of peptide treatments, mouse body weights were measured every 4 days. In addition, after euthanizing animals, organs (kidney, heart, liver, lung, and spleen) were expanded, fixed in 10% neutral buffered formalin, paraffin embedded, and stained with hematoxylin-eosin (H&E) for pathological analysis.

Conflict of Interest: The authors declare no competing financial interest.

Acknowledgment. We would like to thank Ms. Theresa Hyejeong Choi for her help with FACS analysis. The work was supported by the NIH Director's Innovator Award [(1DP20D006462-01), K.B.L.], National Institute of Biomedical Imaging and Bioengineering of the NIH [1R21NS085569-01], the N.J. Commission on Spinal Cord grant [09-3085-SCR-E-0], and the Rutgers Faculty Research Grant Program.

Supporting Information Available: Additional figures as described in the text. These materials are available free of charge *via* the Internet at http://pubs.acs.org.

REFERENCES AND NOTES

1. Chow, E. K.; Ho, D. Cancer Nanomedicine: From Drug Delivery to Imaging. *Sci. Transl. Med.* **2013**, *5*, 216rv214.
2. Ferrari, M. Cancer Nanotechnology: Opportunities and Challenges. *Nat. Rev. Cancer* **2005**, *5*, 161–171.
3. Duncan, R. The Dawning Era of Polymer Therapeutics. *Nat. Rev. Drug Discovery* **2003**, *2*, 347–360.
4. Kievit, F. M.; Zhang, M. Cancer Nanotheranostics: Improving Imaging and Therapy by Targeted Delivery across Biological Barriers. *Adv. Mater.* **2011**, *23*, H217–247.
5. Torchilin, V. P.; Lukyanov, A. N. Peptide and Protein Drug Delivery to and into Tumors: Challenges and Solutions. *Drug Discovery Today* **2003**, *8*, 259–266.
6. Sugahara, K. N.; Teesalu, T.; Karmali, P. P.; Kotamraju, V. R.; Agemy, L.; Greenwald, D. R.; Ruoslahti, E. Coadministration of a Tumor-Penetrating Peptide Enhances the Efficacy of Cancer Drugs. *Science* **2010**, *328*, 1031–1035.
7. Langer, R. Drug Delivery and Targeting. *Nature* **1998**, *392*, 5–10.
8. Hail, N. Mitochondria: A Novel Target for the Chemoprevention of Cancer. *Apoptosis* **2005**, *10*, 687–705.
9. Solary, E.; Bettaieb, A.; Dubrez-Daloz, L.; Corcos, L. Mitochondria as a Target for Inducing Death of Malignant Hematopoietic Cells. *Leuk. Lymphoma* **2003**, *44*, 563–574.
10. Green, D. R.; Kroemer, G. The Pathophysiology of Mitochondrial Cell Death. *Science* **2004**, *305*, 626–629.
11. Green, D. R.; Reed, J. C. Mitochondria and Apoptosis. *Science* **1998**, *281*, 1309–1312.
12. Zhou, F. F.; Wu, S. N.; Wu, B. Y.; Chen, W. R.; Xing, D. Mitochondria-Targeting Single-Walled Carbon Nanotubes for Cancer Photothermal Therapy. *Small* **2011**, *7*, 2727–2735.
13. D'Souza, G. G. M.; Wagle, M. A.; Saxena, V.; Shah, A. Approaches for Targeting Mitochondria in Cancer Therapy. *Biochim. Biophys. Acta: Bioenerg.* **2011**, *1807*, 689–696.
14. Fulda, S.; Galluzzi, L.; Kroemer, G. Targeting Mitochondria for Cancer Therapy. *Nat. Rev. Drug Discovery* **2010**, *9*, 447–464.
15. Chen, W. H.; Xu, X. D.; Luo, G. F.; Jia, H. Z.; Lei, Q.; Cheng, S. X.; Zhuo, R. X.; Zhang, X. Z. Dual-Targeting Pro-Apoptotic Peptide for Programmed Cancer Cell Death *via* Specific Mitochondria Damage. *Sci. Rep.* **2013**, *3*.
16. Constance, J. E.; Lim, C. S. Targeting Malignant Mitochondria with Therapeutic Peptides. *Ther. Delivery* **2012**, *3*, 961–979.
17. Ko, J. K.; Choi, K. H.; Pan, Z.; Lin, P. H.; Weisleder, N.; Kim, C. W.; Ma, J. The Tail-Anchoring Domain of Bfl1 and Hccs1 Targets Mitochondrial Membrane Permeability to Induce Apoptosis. *J. Cell Sci.* **2007**, *120*, 2912–2923.
18. Ko, J. K.; Choi, K. H.; Peng, J.; He, F.; Zhang, Z.; Weisleder, N.; Lin, J. L.; Ma, J. J. Amphipathic Tail-Anchoring Peptide and Bcl-2 Homology Domain-3 (BH3) Peptides from Bcl-2 Family Proteins Induce Apoptosis through Different Mechanisms. *J. Biol. Chem.* **2011**, *286*, 9038–9048.
19. De, G.; Ko, J.-K.; Tan, T.; Zhu, H.; Li, H.; Ma, J. Amphipathic Tail-Anchoring Peptide Is a Promising Therapeutic Agent for Prostate Cancer Treatment. *Oncotarget [Online]* **2014**, *5*.
20. Jacotot, E.; Deniaud, A.; Borgne-Sanchez, A.; Touat, Z.; Briand, J. P.; Le Bras, M.; Brenner, C. Therapeutic Peptides: Targeting the Mitochondrion to Modulate Apoptosis. *Biochim. Biophys. Acta: Bioenerg.* **2006**, *1757*, 1312–1323.
21. Tan, M. L.; Choong, P. F. M.; Dass, C. R. Recent Developments in Liposomes, Microparticles and Nanoparticles for Protein and Peptide Drug Delivery. *Peptides* **2010**, *31*, 184–193.
22. Goldberg, M.; Langer, R.; Jia, X. Nanostructured Materials for Applications in Drug Delivery and Tissue Engineering. *J. Biomater. Sci., Polym. Ed.* **2007**, *18*, 241–268.
23. Cho, K. J.; Wang, X.; Nie, S. M.; Chen, Z.; Shin, D. M. Therapeutic Nanoparticles for Drug Delivery in Cancer. *Clin. Cancer Res.* **2008**, *14*, 1310–1316.
24. McCarthy, J. R.; Weissleder, R. Multifunctional Magnetic Nanoparticles for Targeted Imaging and Therapy. *Adv. Drug Delivery Rev.* **2008**, *60*, 1241–1251.
25. Pankhurst, Q. A.; Connolly, J.; Jones, S. K.; Dobson, J. Applications of Magnetic Nanoparticles in Biomedicine. *J. Phys. Appl. Phys.* **2003**, *36*, R167–R181.

26. Wust, P.; Hildebrandt, B.; Sreenivasa, G.; Rau, B.; Gellermann, J.; Riess, H.; Felix, R.; Schlag, P. M. Hyperthermia in Combined Treatment of Cancer. *Lancet Oncol.* **2002**, *3*, 487–497.
27. Shellman, Y. G.; Howe, W. R.; Miller, L. A.; Goldstein, N. B.; Pacheco, T. R.; Mahajan, R. L.; LaRue, S. M.; Norris, D. A. Hyperthermia Induces Endoplasmic Reticulum-Mediated Apoptosis in Melanoma and Non-Melanoma Skin Cancer Cells. *J. Invest. Dermatol.* **2008**, *128*, 949–956.
28. Salah-Eldin, A. E.; Inoue, S.; Tsukamoto, S. E.; Aoi, H.; Tsuda, M. An Association of Bcl-2 Phosphorylation and Bax Localization with Their Functions after Hyperthermia and Paclitaxel Treatment. *Int. J. Cancer* **2003**, *103*, 53–60.
29. Nijhuis, E. H. A.; Le Gac, S.; Poot, A. A.; Feijen, J.; Vermes, I. Bax-Mediated Mitochondrial Membrane Permeabilization after Heat Treatment Is Caspase-2 Dependent. *Int. J. Hyperthermia* **2008**, *24*, 357–365.
30. Song, X. X.; Kim, H. C.; Kim, S. Y.; Basse, P.; Park, B. H.; Lee, B. C.; Lee, Y. J. Hyperthermia-Enhanced Trail- and Mapatumumab-Induced Apoptotic Death Is Mediated through Mitochondria in Human Colon Cancer Cells. *J. Cell Biochem.* **2012**, *113*, 1547–1558.
31. White, M. G.; Saleh, O.; Nonner, D.; Barrett, E. F.; Moraes, C. T.; Barrett, J. N. Mitochondrial Dysfunction Induced by Heat Stress in Cultured Rat CNS Neurons. *J. Neurophysiol.* **2012**, *108*, 2203–2214.
32. Shah, B.; Yin, P. T.; Ghoshal, S.; Lee, K.-B. Multimodal Magnetic Core−Shell Nanoparticles for Effective Stem-Cell Differentiation and Imaging. *Angew. Chem., Int. Ed.* **2013**, *52*, 6190–6195.
33. Charafe-Jauffret, E.; Ginestier, C.; Iovino, F.; Wicinski, J.; Cervera, N.; Finetti, P.; Hur, M. H.; Diebel, M. E.; Monville, F.; Dutcher, J.; *et al*. Breast Cancer Cell Lines Contain Functional Cancer Stem Cells with Metastatic Capacity and a Distinct Molecular Signature. *Cancer Res.* **2009**, *69*, 1302–1313.
34. Plank, C.; Schillinger, U.; Scherer, F.; Bergemann, C.; Remy, J. S.; Krotz, F.; Anton, M.; Lausier, J.; Rosenecker, J. The Magnetofection Method: Using Magnetic Force to Enhance Gene Delivery. *Biol. Chem.* **2003**, *384*, 737–747.
35. Scherer, F.; Anton, M.; Schillinger, U.; Henkel, J.; Bergemann, C.; Kruger, A.; Gansbacher, B.; Plank, C. Magnetofection: Enhancing and Targeting Gene Delivery by Magnetic Force *in Vitro* and *in Vivo*. *Gene Ther.* **2002**, *9*, 102–109.
36. Cherukuri, P.; Glazer, E. S.; Curleya, S. A. Targeted Hyperthermia Using Metal Nanoparticles. *Adv. Drug Delivery Rev.* **2010**, *62*, 339–345.
37. Xu, Z.; Hou, Y.; Sun, S. Magnetic Core/Shell Fe_3O_4/Au and Fe_3O_4/Au/Ag Nanoparticles with Tunable Plasmonic Properties. *J. Am. Chem. Soc.* **2007**, *129*, 8698–8699.
38. Pack, D. W.; Hoffman, A. S.; Pun, S.; Stayton, P. S. Design and Development of Polymers for Gene Delivery. *Nat. Rev. Drug Discovery* **2005**, *4*, 581–593.
39. Liu, Y.; Shipton, M. K.; Ryan, J.; Kaufman, E. D.; Franzen, S.; Feldheim, D. L. Synthesis, Stability, and Cellular Internalization of Gold Nanoparticles Containing Mixed Peptide-Poly(Ethylene Glycol) Monolayers. *Anal. Chem.* **2007**, *79*, 2221–2229.
40. Chen, W. H.; Chen, J. X.; Cheng, H.; Chen, C. S.; Yang, J.; Xu, X. D.; Wang, Y.; Zhuo, R. X.; Zhang, X. Z. A New Anti-Cancer Strategy of Damaging Mitochondria by Pro-Apoptotic Peptide Functionalized Gold Nanoparticles. *Chem. Commun.* **2013**, *49*, 6403–6405.
41. Kim, C.; Shah, B. P.; Subramaniam, P.; Lee, K. B. Synergistic Induction of Apoptosis in Brain Cancer Cells by Targeted Codelivery of Sirna and Anticancer Drugs. *Mol. Pharm.* **2011**, *8*, 1955–1961.
42. Mellinghoff, I. K.; Wang, M. Y.; Vivanco, I.; Haas-Kogan, D. A.; Zhu, S. J.; Dia, E. Q.; Lu, K. V.; Yoshimoto, K.; Huang, J. H. Y.; Chute, D. J.; *et al*. Molecular Determinants of the Response of Glioblastomas to EGFR Kinase Inhibitors. *New Engl. J. Med.* **2005**, *353*, 2012–2024.
43. Agemy, L.; Friedmann-Morvinski, D.; Kotamraju, V. R.; Roth, L.; Sugahara, K. N.; Girard, O. M.; Mattrey, R. F.; Verma, I. M.; Ruoslahti, E. Targeted Nanoparticle Enhanced Proapoptotic Peptide as Potential Therapy for Glioblastoma. *Proc. Natl. Acad. Sci. U.S.A* **2011**, *108*, 17450–17455.
44. von Wallbrunn, A.; Holtke, C.; Zuhlsdorf, M.; Heindel, W.; Schafers, M.; Bremer, C. *In Vivo* Imaging of Integrin Alpha Nu Beta(3) Expression Using Fluorescence-Mediated Tomography. *Euro. J. Nucl. Med. Mol. Imag.* **2007**, *34*, 745–754.
45. Krotz, F.; de Wit, C.; Sohn, H. Y.; Zahler, S.; Gloe, T.; Pohl, U.; Plank, C. Magnetofection - a Highly Efficient Tool for Antisense Oligonucleotide Delivery *in Vitro* and *in Vivo*. *Mol. Ther.* **2003**, *7*, 700–710.
46. Reers, M.; Smiley, S. T.; Mottola-Hartshorn, C.; Chen, A.; Lin, M.; Chen, L. B. Mitochondrial Membrane Potential Monitored by JC-1 Dye. *Methods Enzymol.* **1995**, *260*, 406–417.
47. Salvioli, S.; Maseroli, R.; Pazienza, T. L.; Bobyleva, V.; Cossarizza, A. Use of Flow Cytometry as a Tool to Study Mitochondrial Membrane Potential in Isolated, Living Hepatocytes. *Biochemistry* **1998**, *63*, 235–238.
48. Fang, M. Z.; Liu, C. G.; Song, Y. L.; Yang, G. Y.; Nie, Y.; Liao, J.; Zhao, X.; Shimada, Y.; Wang, L. D.; Yang, C. S. Over-Expression of Gastrin-Releasing Peptide in Human Esophageal Squamous Cell Carcinomas. *Carcinogenesis* **2004**, *25*, 865–871.
49. Jang, J. T.; Nah, H.; Lee, J. H.; Moon, S. H.; Kim, M. G.; Cheon, J. Critical Enhancements of MRI Contrast and Hyperthermic Effects by Dopant-Controlled Magnetic Nanoparticles. *Angew. Chem., Int. Ed.* **2009**, *48*, 1234–1238.
50. Guo, S.; Huang, Y.; Jiang, Q.; Sun, Y.; Deng, L.; Liang, Z.; Du, Q.; Xing, J.; Zhao, Y.; Wang, P. C.; *et al*. Enhanced Gene Delivery and siRNA Silencing by Gold Nanoparticles Coated with Charge-Reversal Polyelectrolyte. *ACS Nano* **2010**, *4*, 5505–5511.